Journal of Zhejiang University SCIENCE A
ISSN 1673-565X (Print); ISSN 1862-1775 (Online)
www.zju.edu.cn/jzus; www.springerlink.com
E-mail: jzus@zju.edu.cn

Science Letters:

Filament geometrical model and nozzle trajectory analysis in the fused deposition modeling process*

Yu-zhen JIN[†1,2], Jia-fan ZHANG[1], Ying WANG[2], Zu-chao ZHU[†‡1,2]

([1]*State Key Laboratory of Fluid Power Transmission and Control, Zhejiang University, Hangzhou 310027, China*)

([2]*Faculty of Mechanical Engineering & Automation, Zhejiang Sci-Tech University, Hangzhou 310018, China*)

[†]E-mail: gracia1101@yahoo.com.cn; zuchaozhu@zju.edu.cn

Received May 6, 2008; Revision accepted Oct. 15, 2008; Crosschecked Dec. 29, 2008

Abstract: The geometrical model of the filament during the fused deposition modeling (FDM) process was firstly proposed based on three different models, tractrix, parabola, and catenary. Comparing with the actual measured filament curves on the Stratasys 1600 FDM machine, it is indicated that the tractrix model had the best agreement with the actual measured curves. With the analytical simulation, the nozzle trajectories in the straight-line deposition road, circle road, and arbitrary continuous curve road were deduced, according to the traxtric based geometrical model of the filament.

Key words: Fused deposition modeling (FDM), Filament geometrical model, Nozzle trajectory
doi:10.1631/jzus.A0820346 **Document code:** A **CLC number:** TH16

INTRODUCTION

The principle of fused deposition modeling (FDM) is based on surface chemistry, thermal energy, and layer manufacturing technology. As shown in Fig.1, filaments of heated thermoplastic (semi-solid state) are extruded from a nozzle that moves onto the platform in the *X*-*Y* plane to form the first layer. The platform is maintained at a lower temperature, so that the thermoplastic quickly hardens. After finishing the first layer, the platform lowers and the extrusion head deposits a second layer upon the first. Then the process is repeated to fabricate the part (Chua *et al*., 2003; Bellini *et al*., 2004). The schematic of the process is described in Fig.1.

The key strength of FDM products and process include the following features: (1) Ease to use: the product and process are easy to use; (2) Multiple, non-toxic modeling materials: Up to five different modeling materials are available, including ABS (acrylonitrile butadiene styrene), casting wax, maleic anhydride styrene (MAHS), elastomers, and polycarbonate; (3) Automatic support generation and breakaway system: the FDM's software can automatically determine if supports are needed, and generate them if needed; (4) Office environment operation: FDM machines can be installed in an office environment; (5) Speed: the FDM modeling process is simple, accurate, and fast.

However, in the FDM process a number of design and deposition parameters, including material column strength, material flexural modulus, material viscosity, position accuracy, road width, deposition speed, volumetric flow rate, tip diameter, envelope temperature, part geometry, and so on, may impact the fabrication process time and surface finish quality (Yan and Gu, 1996). Many researchers have put forward their optimal results for the fabricating parameters. In Han *et al*.(2002; 2003), a tool path-based deposition planning approach was presented, which can ensure layer quality for a specific set of deposition parameters, say position speed, layer thickness, road width, and flow rate. In Tata *et al*.(1998) and Tyberg and Bohn (1998), adaptive slicing by applying the maximal permissive layer thickness for different slabs

‡ Corresponding author

* Project (No. 50576088) supported by the National Natural Science Foundation of China

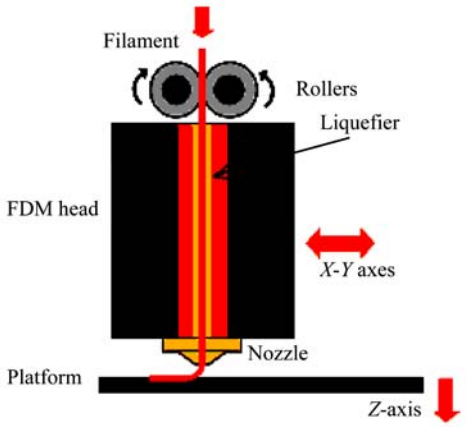

Fig.1 Schematic of FDM

under the constraint of surface finish requirement was used to reduce the build time. In Cheng *et al*.(1995), the optimal parameters, including orientation, road width, layer thickness and source of error during fabrication for stereolithograph were introduced. In Yardimci *et al*.(1996; 1997) and Yardimci (1999), transient heat transfer models were proposed to explain the FD process and understand the rational behind the cooling process.

In this study, three different geometrical models of the filament during the FDM process were firstly analyzed. Then the nozzle trajectories for three classical types of deposition roads were deduced. All experimental investigations were performed on parts made of ABS material and fabricated using the Stratasys 1600 FDM machine (USA). And all simulations were implemented in MATLAB.

GEOMETRICAL MODEL OF THE FILAMENT

The FDM prototypes are an orthotropic composite of ABS filaments, bonding between filaments and voids. They can be viewed and analyzed on different scales. At the macro level, they are studied as laminates of bonded laminar. At the micro level the properties of each laminar are functions of properties of filaments and void density. In this study the principle of the FDM process is in the macro viewpoint. The part is built along with a pre-specified road and each road can be conceptually divided into five segments (Yardmci, 1999): pre-movement, start-up, steady-state, slow-down, and exit-move. Thus, based on the geometrical shape of the filament, we introduced three types of geometrical models of the filament: tractrix, parabola and catenary.

Tractrix model

Fig.2 shows the tractrix model of the filament. According to the properties of the tractrix, assuming the length of the tangent segment between the tangent point $P(x,z)$ on the curve and Z-axis is r. The slope of the tangent line is

$$\frac{\mathrm{d}x}{\mathrm{d}z}=\frac{L}{z}=-\frac{\sqrt{r^2-z^2}}{z}. \tag{1}$$

Taking integration on both sides of Eq.(1):

$$x=-\int\frac{\sqrt{r^2-z^2}}{z}\mathrm{d}z. \tag{2}$$

Substituting z by $r\sin\beta$, and $\cos\beta$ by u,

$$\begin{aligned}x&=-r\int\frac{\cos^2\theta}{\sin\theta}\mathrm{d}\theta=r\int\frac{u^2}{1-u^2}\mathrm{d}u\\&=-\sqrt{r^2-z^2}+r\ln\left|\left(r+\sqrt{r^2-z^2}\right)/x\right|+C.\end{aligned} \tag{3}$$

Note that $0\le z\le r$, so the absolute value is always positive. Therefore, the equation of the tractrix can be given:

$$x=-\sqrt{r^2-z^2}+r\ln\left(\left(r+\sqrt{r^2-z^2}\right)/z\right)+C. \tag{4}$$

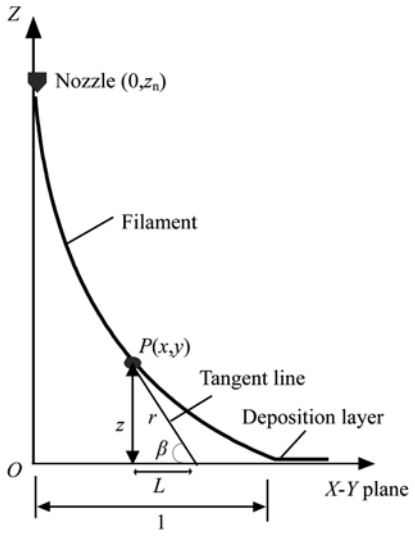

Fig.2 Tractrix model of the filament

According to the characteristic of the tractrix, any tangent segment from the tangent point on the curve to the *Z*-axis has a constant length. So it is noted that at x=0, when z=r, it implies that C=0. And at the start of manufacturing, the height H of the nozzle above the *X*-*Y* platform has been fixed, and is a constant during the fabrication process. So it is easy to conclude that r=H. So Eq.(4) can be rewritten as follows:

$$x=-\sqrt{H^2-z^2}+H\ln\left(\left(H+\sqrt{H^2-z^2}\right)/z\right). \quad (5)$$

Parabola model

For the parabola model, we make the following assumptions: (1) the symmetrical axis of the parabola is x=L; (2) at x=0, z=H.

The equation of the parabola model can be expressed as

$$z=\frac{H}{L^2}(x-L)^2. \quad (6)$$

Catenary model

Similar to the parabola model, the catenary model is given based on the same assumptions. Therefore it is easy to deduce its equation:

$$z=a\cdot\cosh\left(\frac{x-L}{b}\right)+1-H, \quad (7)$$

where coefficients a and b are determined by curve fitting with the measure points of the filament.

Demonstration of the model effectiveness

To demonstrate the feasibility of the geometrical model of the filament, the photo of the filament was taken by a digital camera. And in order to have a precise result, the picture was zoomed to 100 times magnitude to print on a graph paper and sampled at 240 points, in terms of *Z*-axis position from 0 to 0.012 mm (the layer height in the experiment) by step 0.005 mm. From the graph paper, the position of these 240 points on *X* (*Y*)-axis can be measured.

Fig.3 shows the comparison between the actual measured curve and curves of three different models. Obviously, the parabola model is quite different from the actual curve. Though the catenary curve matches much better than the parabola, it is not as good as the tractrix model. Thus, the tractrix model curve matches best to the actual measured curve than the other two curves.

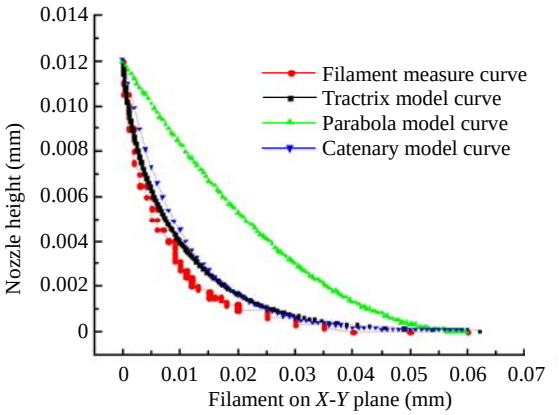

Fig.3 Comparison of the filament measure curve with the three different model curves

Furthermore, it can be found that the actual measured curve is lower than the tractrix model curve, especially at the middle segment of the curve. Besides the measuring errors, the following factors affect the differences between the two curves: (1) The gravity: the gravity of the filament is ignored, when the geometrical model of the filament is built; (2) The surface tension: as the filament is in a semi-solid state when deposited on the platform, it has some characteristics of the liquid. Between the two neighboring layers there is a surface tension bonding the neighboring layers together; (3) The extrusion velocity: the semi-solid thermal plastic is extruded from the tip with the extrusion velocity. The higher the velocity, the lower the curve, and the wider the road.

MATHEMATICAL MODEL FOR THE NOZZLE TRAJECTORY

In the following subsections the trajectory of the nozzle will be given for three regular cases: straight-line road, circle road and arbitrary continuous curve road, based on the filament geometrical model.

Straight-line road

In the FDM process, the most adapted road is straight-line. So as not to lose the generality, it is assumed that the road of the deposition process is a

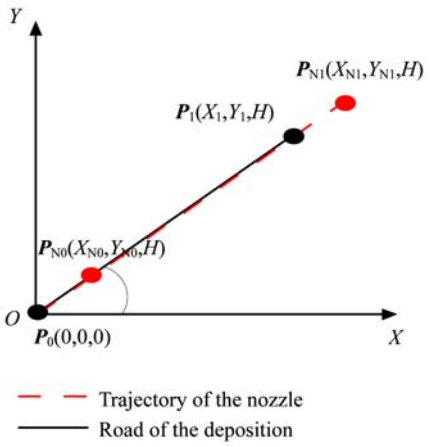

Fig.4 Nozzle trajectory for the straight line deposition road

straight line from point $\boldsymbol{P}_0(0,0,0)$, and the angle between the straight-line and the X-axis is θ (Fig.4). Thus the straight-line road can be expressed as follows:

$$\boldsymbol{P}_i=\{vt\cos\theta, vt\sin\theta, 0\}^{\mathrm{T}}. \tag{8}$$

Through the transformation matrix $\boldsymbol{T}$, the nozzle position can be expressed as follows:

$$\boldsymbol{P}_{\mathrm{N}i}=[\boldsymbol{T}]\cdot\boldsymbol{P}+\boldsymbol{P}_i, \tag{9}$$

where $\boldsymbol{P}=[L\ 0\ H]^{\mathrm{T}}$. Thus,

$$\begin{bmatrix} X_{\mathrm{N}i} \\ Y_{\mathrm{N}i} \\ Z_{\mathrm{N}i} \end{bmatrix}=\begin{bmatrix} \cos\theta & -\sin\theta & 0 \\ \sin\theta & \cos\theta & 0 \\ 0 & 0 & 1 \end{bmatrix}\begin{bmatrix} L \\ 0 \\ H \end{bmatrix}+\begin{bmatrix} vt\cos\theta \\ vt\sin\theta \\ 0 \end{bmatrix}=\begin{bmatrix} (L+vt)\cos\theta \\ (L+vt)\sin\theta \\ H \end{bmatrix}. \tag{10}$$

Substituting the $(L+vt)$ by Vt, where V is the velocity of the nozzle, then Eq.(9) can be written as

$$\boldsymbol{P}_{\mathrm{N}i}=\{Vt\cos\theta, Vt\sin\theta, H\}^{\mathrm{T}}. \tag{11}$$

This is the trajectory of the nozzle for the straight-line deposition road.

Circle road

It is assumed that the circle deposition road is:

$$\boldsymbol{P}_i=\{r\cos\alpha, r\sin\alpha, 0\}^{\mathrm{T}}, \tag{12}$$

where r is the radius of the circle, α is the function of time t.

According to the tractrix model of the filament, the nozzle deposits this road from point $\boldsymbol{P}_{\mathrm{N}0}$ to point $\boldsymbol{P}_{\mathrm{N}m}$ (Fig.5). With the relation between $\boldsymbol{P}_{\mathrm{N}i}$ and $\boldsymbol{P}_i$ in Eq.(9), it has:

$$\boldsymbol{P}_{\mathrm{N}i}=[\boldsymbol{T}]\cdot\boldsymbol{P}+\boldsymbol{P}_i=\begin{bmatrix} \cos\theta & -\sin\theta & 0 \\ \sin\theta & \cos\theta & 0 \\ 0 & 0 & 1 \end{bmatrix}\begin{bmatrix} L \\ 0 \\ H \end{bmatrix}+\begin{bmatrix} r\cos\alpha \\ r\sin\alpha \\ 0 \end{bmatrix}. \tag{13}$$

Obviously, there is the following relation between α and θ:

$$\alpha=\pi/2-\theta. \tag{14}$$

Replacing $\cos\lambda$ by $r/\sqrt{r^2+L^2}$, and $\sin\lambda$ by $r/\sqrt{r^2+L^2}$, then Eq.(14) can be rewritten as

$$\boldsymbol{P}_{\mathrm{N}i}=\begin{bmatrix} \sqrt{r^2+L^2}\cos(\alpha+\gamma) \\ \sqrt{r^2+L^2}\sin(\alpha+\gamma) \\ H \end{bmatrix}=\begin{bmatrix} \sqrt{r^2+L^2}\cos\varphi \\ \sqrt{r^2+L^2}\sin\varphi \\ H \end{bmatrix}, \tag{15}$$

where φ is the function of time t and can be expressed by nozzle velocity V:

$$\varphi=\frac{V}{\sqrt{r^2+L^2}}t. \tag{16}$$

It is apparent that the nozzle trajectory is also just a circle with a larger radius $\sqrt{r^2+L^2}$.

Arbitrary continuous curve road

In this case, the road of the deposition is curve $F(x)$ under the following assumptions: (1) The curve is started from point $\boldsymbol{P}_0(0,0,0)$. (2) The direction of the tangent line at point $\boldsymbol{P}_0(0,0,0)$ is $\boldsymbol{i}$; (3) The curve and its derivative are both continuous.

As analyzed above, the best geometrical model of the filament is the tractrix. So the nozzle extrudes the filament not at point $\boldsymbol{P}_i$, but at $\boldsymbol{P}_{\mathrm{N}i}$ on the

tangent line of the curve $F(x)$ at $\boldsymbol{P}_i$ (Fig.6). The evolution of these tangent lines $\boldsymbol{P}_i\boldsymbol{P}_{Ni}$ is the nozzle trajectory for the curve $F(x)$ deposition road.

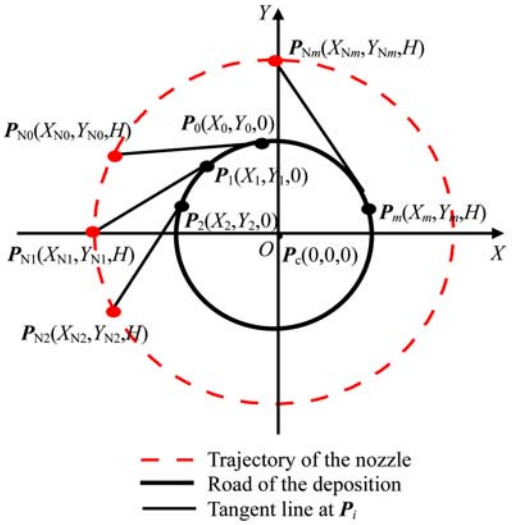

Fig.5 Nozzle trajectory for the circle deposition road

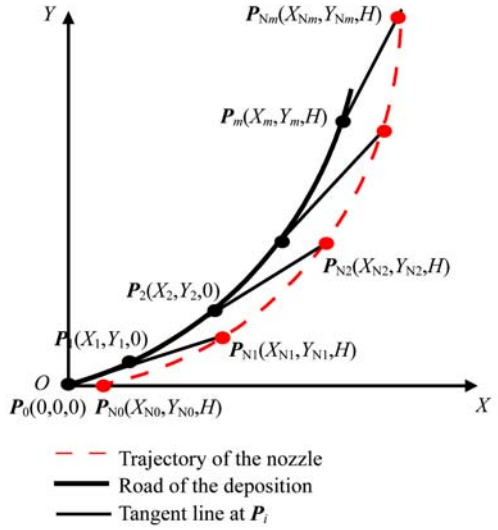

Fig.6 Nozzle trajectory for the curve deposition road

At a random point $\boldsymbol{P}_i$ on the deposition road, the slope of the tangent line is:

$$K_i=\frac{\mathrm{d}y}{\mathrm{d}x}\bigg|_{x=x_i}=\frac{\mathrm{d}F(x)}{\mathrm{d}x}\bigg|_{x=x_i}=F'(x)\big|_{x=x_i}. \quad (17)$$

Thus point $\boldsymbol{P}_{Ni}$ can be calculated as:

$$[\boldsymbol{P}_{Ni}]^{\mathrm{T}}=[\boldsymbol{T}]\cdot[\boldsymbol{P}]^{\mathrm{T}}+[\boldsymbol{P}_i]^{\mathrm{T}}. \quad (18)$$

It can be rewritten in the following form with $\cos\theta=1\Big/\sqrt{1+K_i^2}$, $\sin\theta=K_i\Big/\sqrt{1+K_i^2}$,

$$\begin{bmatrix}X_{Ni}\\Y_{Ni}\\Z_{Ni}\end{bmatrix}=\begin{bmatrix}\cos\theta_i&-\sin\theta_i&0\\\sin\theta_i&\cos\theta_i&0\\0&0&1\end{bmatrix}\begin{bmatrix}L\\0\\H\end{bmatrix}+\begin{bmatrix}X_i\\Y_i\\0\end{bmatrix}=\begin{bmatrix}L\cos\theta_i+X_i\\L\sin\theta_i+Y_i\\H\end{bmatrix}. \quad (19)$$

Thus the points on the imaging curve in the X-Y plane of the nozzle trajectory can be concluded.

For a set of (m+1) points, the spline interpolation is used. The quadratic spline has a sever flaw in that the curvature at the even nodes changes abruptly, leading to an undesired bend or distortion. As a result, we use the piecewise cubic polynomials to overcome this flaw.

In this case we have a position set with (m+1) points and the derivative boundary conditions of the endpoints, which can be obtained from the deposition road. Thus the clamped spline is suitable.

$$\begin{cases}(3h_0/2+2h_1)m_1+h_1m_2=u_1-3(d_0-S'(x_0)),\\h_{i-1}m_{i-1}+2(h_{i-1}+h_i)m_i+h_im_{i+1}=u_i,\\h_{m-2}m_{m-2}+(2h_{m-2}+3h_{m-1}/2)m_{m-1}=u_{m-1}-3(S'(x_m)-d_{m-1}),\end{cases} \quad (20)$$

where $h_i=x_{i+1}-x_i$, $d_i=(y_{i+1}-y_i)/h_i$, $u_i=6(d_i-d_{i-1})$, for i=2, 3, …, m−2.

These equations are easily solved and the result can be expressed for a cubic function $S_i(x)$:

$$S_i(x)=-\frac{m_i}{6h_i}(x_{i+1}-x)^3+\frac{m_{i+1}}{6h_i}(x-x_i)^3+\left(\frac{y_i}{h_i}-\frac{m_ih_i}{6}\right)(x_{i+1}-x)+\left(\frac{y_{i+1}}{h_i}-\frac{m_{i+1}h_i}{6}\right)(x-x_i). \quad (21)$$

Simulation for the nozzle trajectory

In order to verify the mathematical model for the nozzle trajectory, simulations have been performed. In simulations the nozzle height H is still taken as 0.012 mm and L is taken 0.06 mm.

Fig.7a shows the simulation result in the straight-line deposition road case, and Fig.7b for the circle road. Additionally, Fig.7c shows the result of the arbitrary continuous curve deposition road case, in which a polynomial $y=x^4+x^3+x^2+x$ is selected. From the comparison of the nozzle trajectory and the deposition road in each of the three cases, there is a small difference between the two curves.

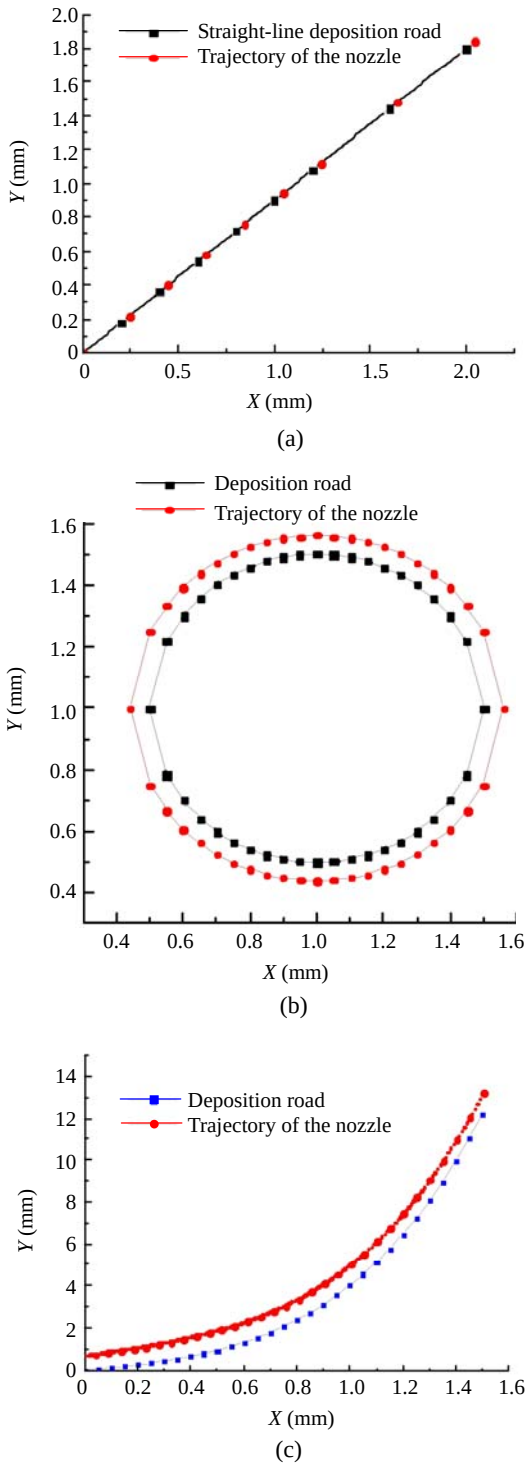

Fig.7 Simulation of the nozzle trajectory. (a) Straight-line deposition road; (b) Circle deposition road; (c) Continuous curve deposition road

CONCLUSION AND FUTURE WORK

In this paper, three kinds of geometrical models (tractrix model, parabola model, and catenary model) of the filament in the FDM process were proposed. The equations of these three kinds of models were deduced. To demonstrate the feasibility, the digital photos have been taken and zoomed to 100 times magnitude for precise measurement. By comparing curves, it showed that tractrix model has the best agreement for the actual measured curve. In addition, the nozzle trajectories in the straight-line deposition road, circle road and arbitrary continuous curve road were analyzed, respectively, based on the geometrical model of the filament.

In the future work, the results of this study will be used to improve the existing working parameters, such as manufacturing accuracy. Additionally, more work concerning kinematics, dynamics and thermal analysis will be developed as a result of this study and the influence of the gravity, surface tension, etc., will be considered more precisely.

References

Bellini, A., Güceri, S., Bertoldi, M., 2004. Liquefier dynamics in fused deposition. *Journal of Manufacturing Science and Engineering*, **126**(2):237-246. [doi:10.1115/1.1688377]

Cheng, W., Fuh, Y.H., Nee, A.Y.C., Wong, Y.S., Loh, H.T., Miyazawa, T., 1995. Multi-objective optimization of part-building orientation in stereolithograph. *Rapid Prototyping Journal*, **1**(4):12-23. [doi:10.1108/13552549510104429]

Chua, C.K., Leong, K.F., Lim, C.S., 2003. Rapid Prototyping—Principles and Applications (2nd Ed.). World Scientific Publishing Co. Pte. Ltd., Singapore.

Han, W., Jafari, M.A., Danforth, S.C., Safari, A., 2002. Tool path-based deposition planning in fused deposition processes. *Journal of Manufacturing Science and Engineering*, **124**(2):462-472. [doi:10.1115/1.1455026]

Han, W., Jafari, M.A., Seyed, K., 2003. Process speeding up via deposition planning in fused deposition-based layered manufacturing processes. *Rapid Prototyping Journal*, **9**(4):212-218. [doi:10.1108/13552540310489596]

Tata, k., Fadel, G., Baghi, A., Aziz, N., 1998. Efficient slicing for layered manufacturing. *Rapid Prototyping Journal*, **4**(4):151-167. [doi:10.1108/13552549810239003]

Tyberg, J., Bohn, J.H., 1998. Local adaptive slicing. *Rapid Prototyping Journal*, **4**(3):118-127. [doi:10.1108/13552549810222993]

Yan, X., Gu, P., 1996. A review of rapid prototyping technologies and systems. *Computer-Aided Design*, **28**(4):307-318. [doi:10.1016/0010-4485(95)00035-6]

Yardimci, M.A., 1999. Process Analysis and Development for Fused Deposition. PhD Thesis, University of Illinois at Chicago, Chicago.

Yardimci, M.A., Hattori, T., Güceri, S., 1996. Conceptual framework for the thermal process modeling of fused deposition. *Rapid Prototyping Journal*, **2**(2):26-31. [doi:10.1108/13552549610128206]

Yardimci, M.A., Hattori, T., Güceri, S., Danforth, S.C., 1997. Thermal Analysis of Fused Deposition. Proceedings of the Solid Freeform Fabrication Symposium, Austin, p.689-698.